Carbohydrate Polymers 117 (2015) 286–296

Contents lists available at ScienceDirect

Carbohydrate Polymers

journal homepage: www.elsevier.com/locate/carbpol

Tunicate cellulose nanocrystals: Preparation, neat films and nanocomposite films with glucomannans

Yadong Zhao, Yujia Zhang, Mikael E. Lindström, Jiebing Li*

Department of Fibre and Polymer Technology, Royal Institute of Technology, KTH, Teknikringen 56-58, SE-100 44 Stockholm, Sweden

ARTICLE INFO

Article history:
Received 21 February 2014
Received in revised form 4 May 2014
Accepted 12 September 2014
Available online 22 September 2014

Keywords:
Tunicate cellulose
Ciona intestinalis
Nanocrystals
Konjac glucomannan
Spruce glucomannan
Nanocomposite films

ABSTRACT

Cellulose nanocrystals (CNs) were prepared from tunicate by enzymatic hydrolysis (ECN), TEMPO-mediated oxidation (TCN) and acid hydrolysis (ACN). They were cast alone or blended with glucomannan (GM) from konjac or spruce to prepare films. Different CNs were obtained with a yield of ECN > TCN > ACN with corresponding order of decreased M_w but increased crystallinity. The CNs' diameters were on the nanometre scale, with lengths of ECN > TCN > ACN. For CN-films, TCN and ACN fibrils were stretched and parallel to each other due to surface charges. For CN–GM films, both components interacted strongly with each other, resulting in changes of crystallinity, specific surface area, fibril diameter and contact angle compared with CN films. The composite films had good thermal, optical and mechanical properties; the last ones are apparently better than similar films reported in the literature. This is the first systematic study of different tunicate CN–GM nanocomposite films and the first ever for spruce GM.

1. Introduction

In recent years, renewable, sustainable and environmentally friendly materials have gained much attention for science and technology development. Among all natural polymers, cellulose is considered to be one of the most promising materials due to its abundant availability in nature and its excellent renewability. Its inherent fibrous and crystal structure makes cellulose attractive for various potential material applications, such as films or composites, due to its high strength, stiffness, transparency and protective barrier. Specifically, cellulose is a good candidate for substituting synthetic polymers for food applications, such as packaging and other food contact surfaces (Sorrentino, Gorrasi, & Vittoria, 2007). Because cellulose is nontoxic and biodegradable, it is particularly advantageous for these applications. For example, cellulose-based edible films have been tested for packaging fresh beans and strawberries (Ayranci & Tunç, 1997). Regenerated cellulose films are biodegradable in soil (Zhang et al., 1996). However, the primary issues remain concerning cellulose applications: processing, performance and cost (Sorrentino et al., 2007). Distinctly, cellulose has very low film formation processability due to its poor dissolution and suspension properties in water. To prepare high performance films or biocomposites, good dispersion in an aqueous solution during processing and strong interactions in the final structures are important. For decades, the degradation of cellulose into nanoscale particles, termed cellulose nanocrystals (CNs), has been an effective means of modifying cellulose. After size reduction, with or without the introduction of surface charge, a CN can be suspended in aqueous solution, improving its processability. In addition, due to its nanometre-size after dispersion, markedly improved mechanical, thermal, barrier and other physio-chemical properties can be obtained for CN fibril films and composites compared to untreated cellulose. In the literature, there are many synonyms used to describe the CNs used in this study, including cellulose microcrystals, whiskers, nanoparticles, microcrystallites, nanofibres, or nanowires. A detailed description of CNs and the field in general may be found in numerous reviews (Azizi Samir, Alloin, & Dufresne, 2005; de Souza Lima & Borsali, 2004; Fleming, Gray, & Matthews, 2001; Habibi, Lucia, & Rojas, 2010; Klemm, Heublein, Fink, & Bohn, 2005; Moon, Martini, Nairn, Simonsen, & Youngblood, 2011; Peng, Dhar, Liu, & Tam, 2011) and textbook (Kimura & Itoh, 2007).

Abbreviations: TC, tunicate cellulose; CN, cellulose nanocrystal; ECN, CN from enzymatic hydrolysis; TCN, CN from TEMPO-mediated oxidation; ACN, CN from acid hydrolysis; GM, glucomannan; KGM, konjac glucomannan; SGM, spruce glucomannan; EKG20, composite film with ECN and 20% KGM; TKG20, composite film with TCN and 20% KGM; AKG20, composite film with ACN and 20% KGM; CSG10, composite film with regenerated TC and 10% SGM; ESG20, composite film with ECN and 20% SGM; TSG20, composite film with TCN and 20% SGM; ASG20, composite film with ACN and 20% SGM; CKG10, composite film with regenerated TC and 10% KGM.

* Corresponding author.
E-mail address: jbing@kth.se (J. Li).

http://dx.doi.org/10.1016/j.carbpol.2014.09.020
0144-8617/

CNs are prepared by various physical and chemical methods, among which acid hydrolysis is the most common (Anglès & Dufresne, 2000; Chang, Wang, Hung, & Perng, 2010; Jiang & Hsieh, 2013). Other methods include mechanical refining (Jiang & Hsieh, 2013), TEMPO-mediated oxidation (Habibi, Chanzy, & Vignon, 2006; Okita, Fujisawa, Saito, & Isogai, 2010a) and enzymatic hydrolysis-assisted mechanical treatment (Henriksson, Henriksson, Berglund, & Lindström, 2007), and these methods produce a suspension of rod-like whiskers whose dimensions depend on the pretreatment method and cellulose origin (de Souza Lima & Borsali, 2004). In principle, the acid hydrolysis can not only remove the amorphous part and shorten the length of the cellulose fibrils, but also introduce charged sulfate groups to the cellulose surface, and increase thus the dispersion ability of the CN in water (Revol, Bradford, Giasson, Marchessault, & Gray, 1992). However, it has also disadvantages, such as that the sulfate moieties at the CN surfaces are labile which can be readily removed with mild alkaline treatment (Habibi et al., 2006). The TEMPO-mediated oxidation converts the hydroxyl groups at the surface of the cellulose into charged carboxyl groups without the liability problem as the sulfate groups (Okita, Saito, & Isogai, 2010b). However, both methods are based on chemical reactions. An enzymatic hydrolysis is a totally bio-based treatment, which has advantages from the environmental point of view when compared with the chemical methods (Henriksson et al., 2007). To our best knowledge, it is rare that all these three methods were used and comprehensively compared in one study.

Among all natural cellulose sources, tunicate is the only animal species that produces cellulose in the outer tissues, termed tunic, from which a purified fraction termed tunicin can be obtained (Hirose, Kimura, Itoh, & Nishikawa, 1999). Similar to plant cellulose, tunicate cellulose (TC) in the tunic aggregates in the form of microfibrils composed of a nearly pure cellulose I_β allomorph (Kimura, Ohshima, Hirose, Nishikawa, & Itoh, 2001). TC has a very large aspect ratio (length = 100 nm to several micrometres and width = 15–30 nm); thus, the aspect ratio is between 3 and 67 (Peng et al., 2011). TC also has a high specific surface area (150–170 m^2/g), a high crystallinity (95%) and a reactive surface due to the presence of hydroxyl groups, which are important for its excellent mechanical properties (Šturcová, Davies, & Eichhorn, 2005). Therefore, TC is an excellent candidate for CN preparation and for film or composite film applications. For example, a tunicin whisker/plasticised starch nanocomposite material has been developed (Anglès & Dufresne, 2000, 2001).

When producing CN-based biodegradable films, synthetic plasticisers are commonly used to further improve their chemical or physical properties, but it was found that for a low molecular weight plasticiser, the plasticiser was easily lost during utilisation, leading to contamination. A better method to achieve this goal is the incorporation of high molecular weight synthetic or natural polymers with cellulose to improve plasticity. Epoxy polymer (Ruiz, Cavaillé, Dufresne, Graillat, & Gérard, 2001), chitosan (Fernandes et al., 2010), starch (Teixeira et al., 2009), xylan (Stevanic, Bergström, Gatenholm, Berglund, & Salmén, 2012), latex (Favier et al., 1995) and PHA latex (Dufresne, Kellerhals, & Witholt, 1999) have been tested. In some cases, the role of CNs is simply to serve as a filler in films (Veigel, Müller, Keckes, Obersriebnig, & Gindl-Altmutter, 2011). A structural analogue to cellulose, glucomannan (GM), is another biopolymer consisting of β-1,4 linked mannose and glucose residues. Due to its low isolation cost, renewability and biodegradability, GM is an attractive candidate to replace traditional artificial polymers (Persson, Nordin, Zacchi, & Jonsson, 2007). Konjac is a well-known source for GM and konjac glucomannan (KGM) has commonly a weight average molecular weight of 1.088×10^6 (Li & Xie, 2006) and a mannose to glucose ratio of 1.51:1 (Yuan, Wu, Zhao, Wu, & Li, 2003). Spruce is another GM-rich source. There are two types of GMs in spruce depending on the galactose content. The spruce glucomannan (SGM) used in this study is the galactose-poor GM and has lower weight average molecular weight (1.0×10^4) and higher mannose to glucose ratio (3.75:1) compared with the KGM (Zhang, Li, Lindström, Stepan, & Gatenholm, 2013). Generally, all mannan-based polysaccharides will interact well with cellulose (Whitney, Brigham, Darke, Reid, & Gidley, 1998), allowing for the production of good composite films from CN and GM blends. In the literature, spruce galactoglucomannan, the galactose-rich GM, and KGM have been used to produce composite films with woody cellulose nanowhiskers (Mikkonen et al., 2010).

The aim of this study was to investigate the performance characteristics, such as high optical and thermal stability, mechanical strength and barrier function, of biodegradable and edible film materials constructed from tunicate CNs with or without the addition of GM to further modify film microstructure and physical properties. Three different preparations of tunicate CNs, enzymatic treatment, TEMPO-mediated oxidation and acid hydrolysis, were applied, and two GMs, KGM and SGM, were included in the study. To our knowledge, this is specifically the first study to report the preparation, structure and high mechanical strength of different tunicate CNs in one study and their forming nanocomposite films with GM and the first ever using SGM in the field.

2. Experimental

2.1. Materials

TC was prepared and characterised from *Ciona intestinalis* in our laboratory (Zhao & Li, 2014). Food additive grade KGM (M_w of 1000k) was purchased from Hubei Konson Konjac Gum Co., Ltd, China. SGM (M_w of 10k) was extracted and purified from spruce (*Picea abies*) holocellulose in our laboratory, as described previously (Zhang et al., 2013). After analysis, the two GMs were found also differing in their mannose:glucose ratio (3.75 for SGM and 1.46 for KGM). Endoglucanase (Novozym 476) was purchased from Novozymes AS (Denmark) and used without further purification. All reagents were of analytical grade, and they were obtained from VWR International AB, Stockholm, Sweden.

2.2. Preparation of CNs

2.2.1. Enzymatic hydrolysis

A 0.5% cellulose suspension in phosphate buffer (pH 5) was prepared. After the addition of Novozym 476 (20 FPU/g), the mixture was incubated at 50 °C for 2 h with shaking manually once every 30 min. The Novozym 476 in the reaction system was then denatured at 80 °C for 30 min. Next, the treated cellulose was recovered by vacuum filtration and washed several times with deionised water (Henriksson et al., 2007). Finally, the tunicate CN was dispersed in deionised water to produce a 0.5% suspension, which was then subjected to homogenisation using an IKA T-25 ULTRA-TURRAX Digital Homogeniser at 15000 rpm for 2 min and ultrasonication (Unique Sonicator, 40 kHz) for 1 min in an ice-bath to yield a homogeneous CN suspension, termed ECN.

2.2.2. TEMPO-mediated oxidation

Cellulose (0.5 g) was suspended in water (100 ml) containing TEMPO (0.016 g, 0.1 mmol) and sodium bromide (0.1 g, 1 mmol). The cellulose suspension was stirred continuously at 400–500 rpm. Then, 3.1 ml aqueous NaClO solution (12%, ~1.61 M, made from the commercial NaClO with a commercially described 10–15% available amount of chlorine) was added drop-wise, so the total addition of NaClO was ~5 mmol, equivalent to 10 mmol per gram of cellulose (Okita et al., 2010b). The pH of the reaction system was controlled at 10.0 ± 0.1 via the addition of 0.5 M NaOH. The reaction reached

completion when no further change in pH was observed, and it was fully quenched by the addition of 100 ml of ethanol (Okita et al., 2010a). The oxidised cellulose was recovered by vacuum filtration and washed several times with ultrapure water to obtain a neutral pH. Then, a 0.5% homogeneous suspension of the TEMPO-mediated oxidised cellulose fibres in water was prepared as mentioned above using the blender-type homogeniser at 15,000 rpm for 2 min, followed by ultrasonication for 1 min to produce TCN.

2.2.3. Acid hydrolysis

A 0.5% cellulose suspension was prepared in 55% (v/v) H_2SO_4 solution and hydrolysed at 60 °C for 20 min with vigorous stirring. Then, the suspension was subjected to high-speed centrifugation (20,000 × *g*) for 15 min, and the precipitate was washed three times with 100 ml of deionised water by re-dispersion and re-centrifugation (Anglès & Dufresne, 2000). Finally, the tunicate CN was dispersed in the deionised water to produce a 0.5% suspension, which was homogenised and sonicated to form the CN suspension as mentioned above, termed ACN.

2.3. Preparation of neat CN films and CN–GM composite films

The CNs prepared above were directly cast on Petri dishes (15 ml with ~75 mg solid content onto a 21 cm^2 area) and dried at 50 °C overnight to make neat CN films. The thickness of the films was approximately 10–20 μm.

For CN–GM composite films, a 0.5% KGM or SGM solution/suspension was prepared by adding KGM or SGM in deionised water at 80 °C. The composite films were then prepared by adding the designated amount of CN to KGM or SGM. After mixing the KGM/SGM with the aqueous CN suspension by magnetic stirring at 80 °C for 5 min, the mixed suspension was cast on Petri dish to obtain films (15 ml with ~75 mg solid content onto a 21 cm^2 area). The films were dried at 50 °C overnight. The resulting films (10–20 μm thick) were termed AKG or ASG, EKG or ESG and TKG or TSG, followed by a number indicating the GM addition percentage after blending ACN, ECN and TCN, respectively, with KGM or SGM. For example, EKG 20 denotes an ECN–KGM film made by blending 80% ECN and 20% KGM.

As a reference experiment, the starting TC was immersed in ionic liquid containing 1-butyl-3-methylimidazolium chloride (BmimCl) and stirred at 90 °C for at least 3 h (until dissolved) to prepare a 0.5% solution, and KGM/SGM was also dissolved in BmimCl to prepare a 0.5% solution. The obtained solutions were mixed to produce blend mixture solutions having different TC to GM mass ratios, as described previously. The blend mixture solutions were stirred energetically for more than 3 h, degassed at 60 °C, and spread over a Petri dish to form a film (15 ml with ~75 mg solid content onto a 21 cm^2 area). The Petri dish covered with the blend solution was coagulated with distilled water until the film detached. The detached film was immersed in running water for over 12 h and then dipped in deionised water three times (over 3 h every time) with slight stirring to completely remove BmimCl. Finally, the transparent films were dried at 50 °C overnight, and they were named CKG or CSG, followed by a GM addition percentage number.

2.4. Characterisation methods

2.4.1. Size exclusive chromatography (SEC) analysis

First, TC and CNs (30 mg) were activated with 30 ml of deionised water at 4 °C for 1 h, and the excess water was removed by filtration. Next, solvent-exchange with methanol (30 ml) was applied three times, followed by *N*,*N*-dimethylacetamide (DMAc) (30 ml) for 30 min. The activated samples were then dissolved in 8% LiCl/DMAc to reach a concentration of 0.8% of the sample weight by stirring at 4 °C for 5 days, and the solutions were diluted with DMAc to reach a final concentration of 0.5% with respect to sample weight. The SEC system was equipped with a Rheodyne injector, a DGU-20A3 degasser, a LC-20AD liquid chromatography system and a RID-10A refractive index detector. The separations were achieved using four 20 μm Mixed-A columns with a guard column. The injection volume was 100 μl, and the separations were performed at 80 °C with the flow rate of 0.5 ml/min of 0.5% LiCl/DMAc. Calibration was conducted with pullulan standards of nominal masses ranging from 320 to 800 kDa (Fluka/Riedel-de Haën, Seelze, Germany). Data acquisition and analysis was performed using LC Solution software (Shimadzu, Kyoto, Japan) equipped with the SEC system.

2.4.2. Morphological analysis

Before scanning electron microscopy (SEM) analysis, all samples were coated with gold using a Cressington 208HR high-resolution sputter coater. A Cressington thickness monitor controller was used to control the thickness (3–5 nm). Then, sample morphology was analysed using a Hitachi S-4800 Field Emission Scanning Electron Microscope.

The morphology of the cellulose nanocrystals was imaged with tapping-mode AFM (Multimode IIIa, Veeco, Santa Barbara, CA). The AFM images were recorded under ambient and air conditions (23 °C and 50% relative humidity). RTESP silica cantilevers (Veeco) having a tip with a radius of 8 nm and a spring constant of 40 N/m oscillated at their fundamental resonance frequencies between 200 and 400 kHz.

2.4.3. Z-potential determination

The zeta potential of the cellulose suspensions was measured using a Zetasizer Nano Z system (Malvern Instruments, UK). A nanocrystalline cellulose suspension (0.05%), previously sonicated for 5 min, was prepared and analysed to determine the zeta potential of the CN suspensions.

2.4.4. Thermo gravimetric analysis (TGA)

Thermo gravimetrical analysis was collected using a Mettler Toledo TGA/SDTA 851^e equipped with STAR^e software for data analysis. The samples were subjected to a heating scan between 30 and 800 °C, with a rate of 10 °C/min under an inert atmosphere of nitrogen at a gas flow of 50 ml/min.

2.4.5. Fourier transform infrared spectroscopy (FTIR) analysis

Fourier transform infrared spectra were obtained using a Perkin-Elmer Spectrum 2000 FTIR spectrometer (Waltham, MA, USA) equipped with an ATR system, Spectac MKII Golden Gate (Creecstone Ridge, GA, USA). The samples were analysed at wavelengths ranging from 600–4000 cm^{-1}. All spectra were obtained from dry samples subjected to 16 scans at a resolution of 4 cm^{-1} and an interval of 1 cm^{-1} at room temperature. Before data collection, background scanning was performed for background correction. Dynamic FTIR (Fourier transform infrared) spectra were recorded on a Varian 680-IR spectrometer (Varian Inc., Santa Clara, CA, USA) in transmission mode with a liquid nitrogen cooled MCT (Mercury Cadmium Telluride) detector. Thin films were mounted between two parallel jaws in a specially constructed polymer modulator (PM-100) which was placed in a temperature control system (TC-100) (MAT-Manning Applied Technology Inc., Troy, ID, USA). A modular humidity generator (MHG-32) (Projekt Messtechnik, Ulm, Germany) was connected to the TC-100. The average in-phase and out-of-phase spectra were made and normalised as described in detail in the literature (Stevanic et al., 2012).

2.4.6. X-ray diffraction (XRD) analysis

A PANalytical X'Pert PRO Materials Research Diffractometer equipped with an X'Celerator detector was used to determine

the crystallinity index (CI) of the samples. The analysis was performed using monochromatic Cu$K\alpha$ radiation at 30 mA and 40 kV. CI, defined to evaluate the crystallinity of the different samples, was calculated using the following equation:

$$\mathrm{CI} = \frac{I_{200} - I_{am}}{I_{200}} \times 100$$

where I_{200} is the intensity of the 200 lattice plane at $2\theta = 22.8^\circ$, and I_{am} is the intensity from the amorphous phase at approximately $2\theta = 18^\circ$ (Reddy & Yang, 2005).

2.4.7. Specific surface area analysis

The analysis was conducted by measuring the gas adsorption properties of the sample for which a BET-analysis was performed. First, approximately 0.1 g of sample was heated and degassed at 115 °C under a vacuum for >300 min, removing all foreign adsorbed molecules. Then, controlled amounts of an inert gas (nitrogen) were introduced and adsorbed. At the temperature of liquid nitrogen (−196 °C), the sample was exposed to varying pressures to generate adsorption isotherms. Adsorbed amounts were determined by the pressure variations due to adsorption by the sample. A Micrometritics ASAP 2020 Surface Area and Porosity Analyzer (Micromeritics, USA) and its software were used.

2.4.8. Contact angle determination

The contact angle (CA) was determined by the pendant drop method with a water drop and an optical contact angle meter SL 100B from Solon Information Technology Co., Ltd. (Shanghai, China) at a relative humidity (RH) of 50% and 23 °C. To compare different samples, each contact angle was taken at 45 s, and the average value of at least three measurements was used.

2.4.9. UV–vis transmittance determination

The percent light transmission (T%) of the films was monitored using Shimadzu UV-240 (Japan) equipment. To compare different samples, readings were taken at a wavelength of 600 nm. Film specimens were cut into rectangles and placed in a spectrophotometer test cell directly, and air was used as the reference. Transmittance was used to define the transparency of a measured film. Due to the differences in the film thicknesses, a normalisation procedure was followed to obtain normalised transmittance by thickness from normalised A^* according to Beer–Lambert law using

$$A^* = A \times \frac{l}{l_a}$$

where A is the observed absorbance at the film thickness (μm) of l for the film concerned while l_a (13.2 μm) is the average thickness for all prepared films in this study. That is to say all the transmittances for films were normalised with the same thickness of 13.2 μm and then compared directly.

2.4.10. Mechanical strength measurement

The tensile strength and Young's modulus of the films were determined using an Instron 4411 mechanical property tester with a 500-N load cell (Instron Ltd., Norwood, MA, USA). The initial grip distance was 25 mm, and the rate of grip separation was 5 mm/min. Two films of each type and three specimens from each film were tested. The specimens were 5 mm wide and approximately 60 mm long. The thickness of the specimens was measured at three points using a micrometer (NSK, Japan).

2.4.11. Conductometric titration

The total carboxyl group content of TCN was determined by conductimetric titration according to SCAN-CM 65:02 standard with some modifications as described by other researchers (Araki, Wada, & Kuga, 2000; Habibi et al., 2006; Rusli, Shanmuganathan, Rowan, Weder, & Eichhorn, 2011). Briefly, TCN (100 mg) was suspended in 50 ml of 0.01 M HCl solutions containing 0.01 mM NaCl. After stirring for 10 min, the suspensions were titrated with 0.01 M NaOH. The conductometric titration was performed three times and the average value was used. Finally, the amount of the carboxyl groups was calculated by the following equation:

$$X = \frac{C_t \times V}{m} \times 10^6$$

where X is the total carboxyl group content (μmol/g), C_t is the NaOH concentration (mol/l), V is the amount of NaOH (l) consumed corresponding to the plateau region and m (g) is the weight of the CN in the water suspensions.

The similar conductometric titration was used to determine the acidic group content of ACN (—OSO_3^-) without HCl addition. Briefly, 100 mg ACN was suspended in 50 ml of 0.01 mM NaCl and poured into a 100 ml three-necked round-bottomed flask. Then, the mixture was stirred continuously for 10 min. The suspension was titrated using 0.002 M sodium hydroxide. The surface charges (—OSO_3^-) were calculated from the same equation above though the V here is the volume of NaOH (l) consumed before conductivity increase (Rusli et al., 2011). This method was also used to determine the total acidic groups of ECN.

3. Results and discussion

3.1. CN preparation

The starting TC prepared from *Ciona intestinalis* consisted of large molecules, with an M_w of 7.31×10^5 and a polydispersity index (PDI) of 11.1 (Table 1). The morphology of the TC was similar to its natural form in the original animal in terms of cellulose fibre structure, displaying long cellulose chains tightly packed together in crystallites, stabilised by strong and very complex intra and inter molecular hydrogen bonds, termed cellulose microfibrils. Due to its high molecular mass and compact morphological structure, TC was not soluble or able to be suspended in water. In this study, we utilised the three preparation methods mentioned above, i.e. enzymatic treatment, TEMPO-mediated oxidation and acid hydrolysis to produce CNs from TC to improve its dispersion in water and its ability to be processed using an aqueous solution via molecular mass and morphological size reduction, with or without the introduction of surface charge.

Morphologically, amorphous and crystalline regions were present in the cellulose microfibrils. The crystalline regions are so compact that almost no crystal structure modifications took place at these regions. For enzymatic hydrolysis, Novozym 476, an endoglucanase, was used, which mainly attacked the amorphous regions to shorten the cellulose chains by hydrolysis. TEMPO-mediated oxidation occurred mainly via oxidation of the —CH_2OH groups at the C_6 position, preferably in the amorphous region, which facilitated the mechanical disintegration of the cellulose after the oxidation, resulting in a gentle shortening of the cellulose chains and the introduction of charged carboxylic groups. Sulphuric acid induced a strong hydrolysis that removed a portion of the microfibrils by disrupting the amorphous regions surrounding the embedded parts within the cellulose microfibrils while leaving the microcrystalline segments intact. Simultaneously, charged surface sulphate esters were generated. Comparatively, enzymatic hydrolysis was the mildest (73.4% recovery yield), followed by TEMPO-mediated oxidation (62.8% recovery yield) and acid hydrolysis (30.0% recovery yield) (Table 1).

Table 1
Recovery yield, molecular mass, size, zeta potential and charged group content of the tunicate cellulose nanocrystals (CNs) compared to starting tunicate cellulose (TC).

	TC	ECN	TCN	ACN
Recovery yield (%)	100	73.4	62.8	30.0
Molecular mass				
M_w	731,000	46,300	30,900	5750
M_n	66,000	29,200	21,800	2170
PDI	11.1	1.58	1.42	2.65
Size				
Width (nm)	16.04 ± 0.64	17.1 ± 2.7	15.9 ± 2.0	20.0 ± 2.8
Length (nm)	Several micrometres	Several micrometres	1590 ± 759	694 ± 312
Zeta potential (mV)	–	−7.48	−40.3	−18.3
Charged group content (μmol/g)	–	13.6	428	68.3

3.2. CN structures

The molecular mass of the CNs after enzymatic treatment, TEMPO-mediated oxidation and acid hydrolysis decreased, with ECN > TCN > ACN (M_w of 4.63×10^4, 3.09×10^4 and 5750, respectively). Due to structural modifications, the PDI decreased to 1.42–2.65, indicating that the CNs had more uniform molecular mass distributions compared to the starting TC (Table 1). FTIR analysis revealed that all CNs showed typical cellulose structural characteristics (Fig. 1(A)), with O—H, C—H and C—O stretching vibrations at 3334 cm^{-1}, 2901 cm^{-1} and 1057 cm^{-1}, respectively. The peak at 1638 cm^{-1} was associated with the O—H bending vibration of absorbed water. For ECN, the peak near 1738 cm^{-1} represented the presence of carbon atoms in various oxygen environments (Łojewska, Miśkowiec, Łojewski, & Proniewicz, 2005). For TCN, the pronounced peak at 1609 cm^{-1} indicated an asymmetrical carboxylate COO^- vibration overlapping with the O—H bending vibration of the absorbed water (Jiang & Hsieh, 2013), verifying the presence of charged carboxyl groups introduced by TEMPO-mediated oxidation. Here, the absolute vibration frequency was dependent on the status of the functional groups (Łojewska et al., 2005). For ACN, the significant peak near 1160 cm^{-1} confirmed the presence of charged sulphate ester bonds on the cellulose chains generated by sulphuric acid hydrolysis (Chang et al., 2010).

The contents of charged groups on the CNs were determined by conductometric titrations of aqueous CNs suspensions. The results showed that TCN exhibited a carboxyl group content of 428 μmol/g (Table 1), which agrees quite well with the 300–500 μmol/g reported by Besbes, Alila, and Boufi (2011). It was followed by ACN with a charged group ($-OSO_3^-$) content of 68.3 μmol/g, which was slightly lower than the 85 μmol/g reported by Rusli et al. (2011). It is reasonable to find out the lowest charged group content (13.6 μmol/g) for ECN due to the highly limited surface modification or charge introduction by the enzyme. To evaluate distribution of the charged groups on the surfaces of CNs, zeta potentials of the CNs dispersed in water were investigated (Section 2.4.3). TCN displayed the highest charge density, with a zeta potential of −40.3 mV, and ACN displayed a charge density of −18.3 mV followed by slightly charged ECN (−7.48 mV (Table 1)). The high amount of charged groups and high zeta potential values indicate that the TCN and ACN dispersions in water will be very stable. For ECN, the zeta potential was quite low which confirmed no extra charge introduction by the enzyme. It should be pointed out here that due to the longest length of ECN compared with ACN and TCN

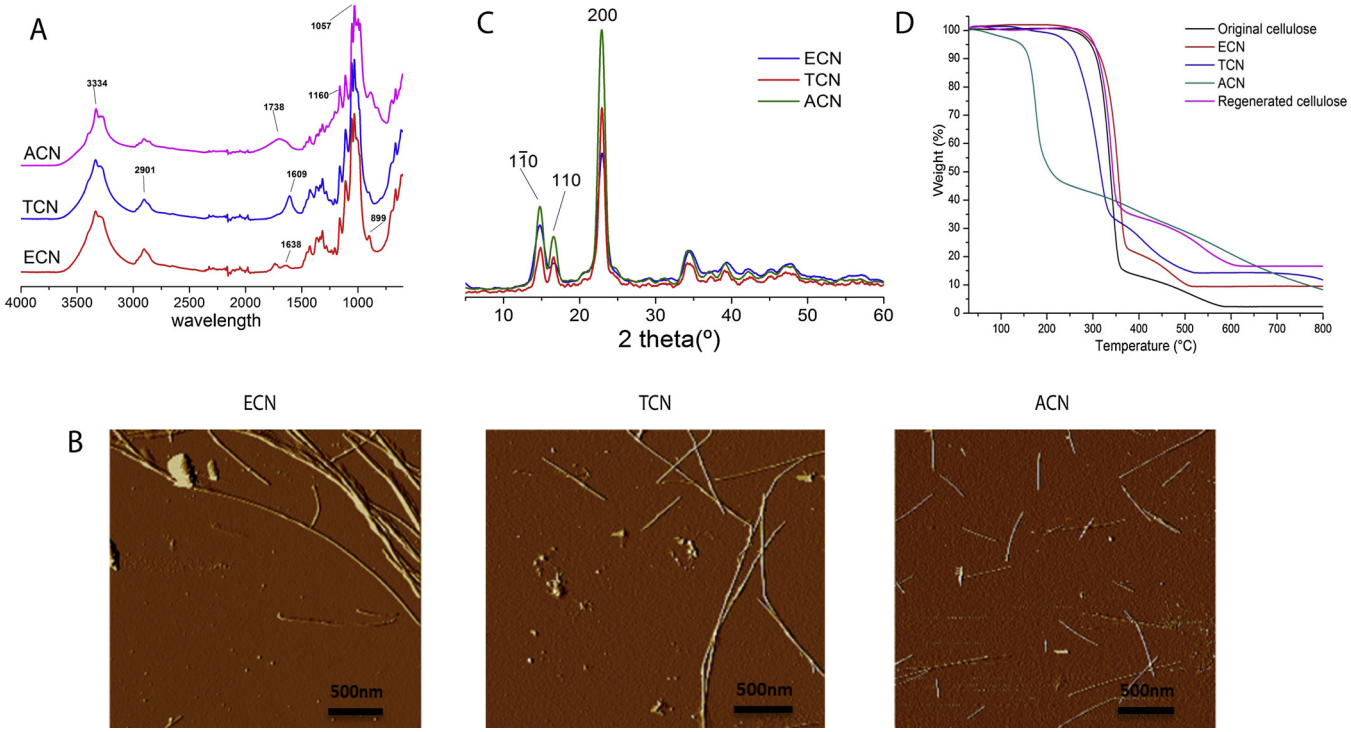

Fig. 1. Characterisation of the freeze-dried cellulose nanocrystals against original cellulose and regenerated cellulose from tunicate. (A) FTIR spectra, (B) AFM images, (C) X-ray diffraction (XRD) patterns and (D) thermal gravimetric analysis (TGA) graphs.

(Table 1), there could be underestimation of the apparent value of zeta potential for ECN because larger particles moved slower. Furthermore, it is noticeable that the order for zeta potentials is consistent to that of charged group contents of CNs. It was confirmed that different methods for preparation of CNs did lead to different charge density and distribution which may thus influence their behaviours in further applications. Obviously the TEMPO oxidation has been demonstrated to be the most effective method to introduce charges onto the surface of CN.

Irrespective of the preparation method used, all of the CNs obtained were rod-like nanocrystals (Fig. 1(B)), displaying nanometre scale diameters, ranging from 15.9 to 20.2 nm. Although no significant difference was observed in the width of the crystals among different CNs, the length decreases in the following order: ECN > TCN > ACN (by several micrometres, 1590 nm and 694 nm, respectively) (Table 1). In the literature, no systematic investigation or comparison has been reported for preparations of different CNs from TC with different methods. Generally, the sizes of TCNs in this study agree quite well with the reported values from different studies, e.g. fibril length of 0.1–10 μm and width of 5–20 nm (Habibi et al., 2006), and the ACN fibrils having 1–2 μm for length and 8–30 nm for width when obtained from other tunicate celluloses (Elazzouzi-Hafraoui et al., 2007; Rusli et al., 2011; Uddin, Araki, & Gotoh, 2011).

All the CNs displayed similar morphology and crystallinity compared to the original TC due to limited modifications at the amorphous domains and the intact crystalline domains. As illustrated in Fig. 1(C), the X-ray diffraction curves of ECN, TCN and ACN displayed a typical cellulose I structure, with strong crystalline peaks at 14.7°, 16.8° and 22.8°, corresponding to the $(1\,\bar{1}\,0)$, (1 1 0), and (2 0 0) crystal planes, respectively. The crystallinity index (CI) increased in the following order: ECN < TCN < ACN (82.8, 87.5 and 90.7%, respectively). Thus, the higher the hydrolysis percentage during the CN preparation, the lower the extent of the remaining amorphous regions, resulting in the shorter length and the higher crystallinity of the CN. This finding could serve as a rule-of-thumb for the preparation of CNs.

Comparatively, ECN has the highest thermal stability, as its decomposition started at approximately 260 °C, the same temperature as for the starting TC (Fig. 1(D)). The decomposition of TCN began at approximately 220 °C, 40 °C lower than ECN, and ACN decomposed at a much lower temperature, ~120 °C. Apparently, the molecular mass is a decisive factor for thermal stability; the higher the M_w, the more thermally stable the CN. Notably, the CN crystallinity is not a decisive factor because the crystal structure in the regenerated TC has been mostly destroyed during the regeneration process but it still displayed good thermal stability.

3.3. CN films

In this study, the basic procedure for making CN films was as follows: CN water suspension – casting – evaporation; this procedure is suitable for water soluble or dispersible polymers. After homogenisation and ultrasonication (see Section 2.2), all CNs were uniformly dispersed, especially TCN and ACN where the charged groups supplied additional electrostatic repulsion that assisted particle dispersion. Due to the dispersions, CN fibrils have ultra-large interfacial areas. After casting in a very dilute concentration (0.5%), the CN fibrils were randomly oriented in the dilute regime, and they arranged themselves as polymer lattices with the lowest repulsion after casting and evaporation. In addition, the evaporation of water tended to cause the CN fibrils to adopt the configuration that minimised electrostatic interactions, especially for TCN and ACN. In other words, the evaporation process was a self-assembly process used by the CN fibrils to form an intermingling network structure. The thickness of the CN films ranged from 10 to 20 μm. The rod-like CN fibrils oriented themselves during network formation, and due to the high charges at the surface of TCN and ACN, the fibrils tended to stretch and align parallel to each other, and this structure was preserved after complete water evaporation to form the film (Fig. 2).

Table 2
Specific surface area (m^2/g) of different neat CN and CN–GM films.

	ECN	TCN	ACN
After freeze drying	161.3	61.7	26.0
Neat CN film	29.0	61.1	63.4
CN–KGM film	18.7 (EKG30)	4.40 (TKG50)	3.70 (AKG50)
CN–SGM film	10.4 (ESG20)	8.71 (TSG50)	3.60 (ASG50)

During film formation, interactions or inter-molecular hydrogen bonds are formed between the CN fibrils as they approach each other. As a reference experiment, the CN suspensions were freeze-dried, and their specific surface areas (SSAs) were measured (Table 2). During freeze-drying, the water evaporated directly from ice without collapsing the structure of the network. Therefore, the SSA reflects the "original" distances between the CN fibrils when no additional interaction was formed between the fibrils. The CNs connected to each other with a SSA spacing of 161.3, 61.7 and 26.0 m^2/g for ECN, TCN and ACN, respectively. In contrast, the ECN film formed after casting-evaporation was obviously denser than the "original" CN fibrils, with a smaller SSA (28.9 vs. 161.3 m^2/g). The TCN film had the similar SSA (61.1 vs. 61.7 m^2/g), while the ACN film was more expanded (63.4 vs. 26.0 m^2/g) (Table 2). Apparently, ECN fibrils tended to aggregate when the film was forming. Due to their high charge, similar aggregations did not occur with TCN or ACN fibrils. The TCN film formed a similar network to that obtained after freeze-drying. For the ACN film, a looser network was formed.

3.4. CN–GM composite films

The procedure of "water suspension–casting–evaporation" was also applied to prepare CN–GM composite films after blending CN with GM during the first step, when GM solution (for KGM) or suspension (for SGM) was added to the CN suspension. Due to similar polysaccharide structures, both CN and GM components display high density hydroxyl groups, which provide their hydrophilic nature and good miscibility and interactions (e.g., hydrogen bonds between the components are expected). After casting and evaporation, they formed the percolation network, with GM functioning as cement to reinforce the CN network in the composite film. The thickness of the composite films ranged from 10 to 20 μm.

The inter-fibril interactions between CN and GM were observed using dynamic FTIR analysis of the EKG20 composite film (Fig. 3) recorded at 0° polarisation, 80% RH and 30 °C; the in-phase spectrum (thin line) indicates elastic responses, and the out-of-phase spectrum (thick line) indicates viscous responses. In the in-phase spectrum, two absorption vibrations are highlighted, one cellulose signal at 1434 cm^{-1} (C—OH bending vibration of the CH_2—OH group attached at glucose unit) and one KGM signal at 813 cm^{-1} caused by the equatorially aligned hydrogen at the C_2 atom in the mannose residue, and they were simultaneously strained by the sinusoidal perturbation (Stevanic et al., 2012; Stevanic & Salmén, 2009). Interestingly, the interactions were observed at 80% RH and it resulted from the hydrogen bonds formed between ECN and KGM.

Because of the strong interactions between CN and GM, the crystallinity index (CI) of the composite films changed, as revealed by XRD analysis (Fig. 4(A)). The CI of all the CN composite films with KGM decreased as the percentage of KGM increased. The strongest interactions were observed for ECN, which was the least charged of all the CNs. The CI for EKG films decreased quickly (from 77% to 37%) when the KGM addition percentage increased from 0 to 50%.

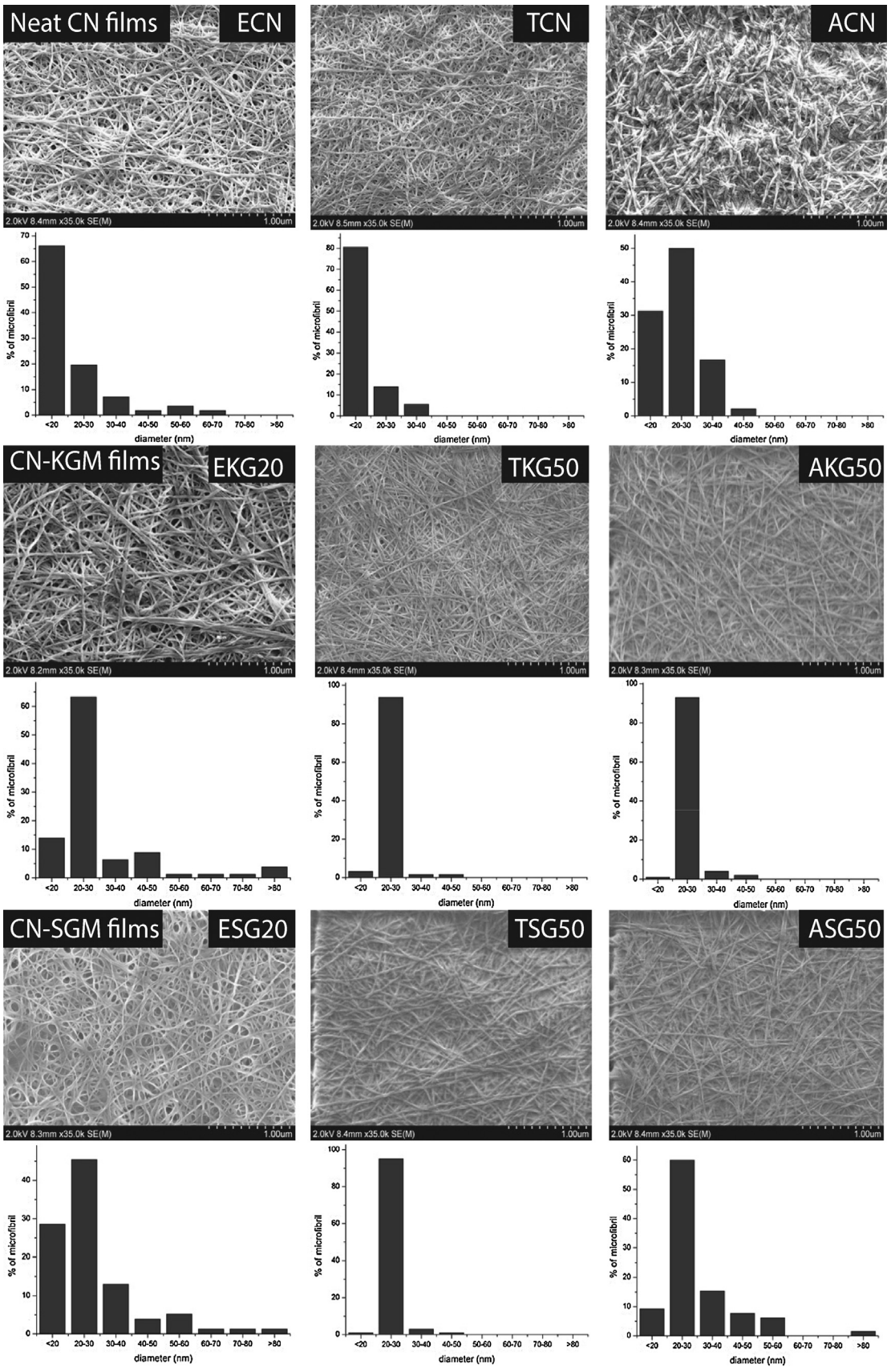

Fig. 2. Surface SEM images and fibril width distribution of CN or CN–GM composite films.

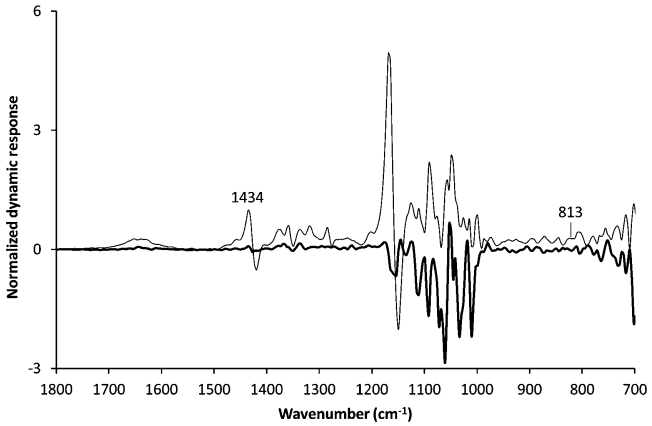

Fig. 3. Dynamic FTIR spectra of EKG20 composite film.

However, the changes for the TCN and ACN films were not significant, except when the KGM percentage increased from 40 to 50% in the ACN composite film. During composite film formation, most of the cellulosic chains were perturbed by the presence of KGM, which decreased the crystallinity, verifying the results of another study (Whitney et al., 1998). In addition, this CI decrease could also be due to the masking effect from the added GM on the diffraction from the crystalline CNs.

The strong interaction between CN and GM was confirmed by measuring the width distribution of the CN microfibrils obtained from 100 measurements from multiple SEM images for each type of CN–GM composite film (Fig. 2). Generally, the addition of GM increased the diameter of the majority of the fibrils. For example, most of the fibrils in the ECN neat film were <20 nm. After the addition of KGM or SGM, the majority of the fibrils had widths of 20–30 nm. Similar changes were observed for TCN and ACN composite films. This diameter increase of CN fibrils could be explained by the aggregation of cellulose and KGM induced by the newly introduced intermolecular hydrogen bonds, as illustrated by the above-mentioned dynamic FTIR, which is consistent with the results of previous studies (Whitney et al., 1998). With identical addition percentages (20, 50 and 50%) in ECN–, TCN– and ACN–GM composites, the diameter increases were more obvious for SGM compared to KGM (Fig. 2), implying stronger interactions between the CNs and SGM compared to KGM.

The cement effect of GM for the composite film network was observed by determining the SSA (Table 2) and contact angle (Fig. 4(B)). After the addition of KGM or SGM, the empty spaces in the neat CN films were cemented with GM, leaving now negligible empty spaces (<20 m^2/g SSA for all CN–KGM and CN–SGM composite films) (Table 2). Moreover, contact angles were stable or slightly increased after increasing the percentage of KGM. The probe liquid for the contact angle test was water, which tended to penetrate into the empty spaces during the assay. Therefore, the less empty space the composite film has, the less water penetration; thus, a stable or slightly larger contact angle will be observed.

Morphologically, TCN– and ACN–GM composite films are very different from ECN–GM composite films due to surface charges, as revealed by SEM analysis (Fig. 2). Again, the presence of charges caused the CN fibrils to align parallel to each other in one layer, and different layers had different orientation directions. This phenomenon is known as chiral nematic order, resulting in optically variable properties (Capadona et al., 2007). In contrast, ECN–GM composite films lacking charge have curved fibril orientation, especially the ECN–SGM film (Fig. 2). The curving is thought to be the result of water evaporation.

3.5. Properties of CN–GM composite films

3.5.1. Thermal stability

Compared to the CNs (Fig. 1(D)), the CN–KGM composite films with different concentrations of KGM showed similar thermal stability (Fig. 4(C)), suggesting that the addition of KGM did not significantly influence their thermal properties. This might be due to the dominant role of CN fibrils in the composite films, while KGM provides only a cement-like function in the structure.

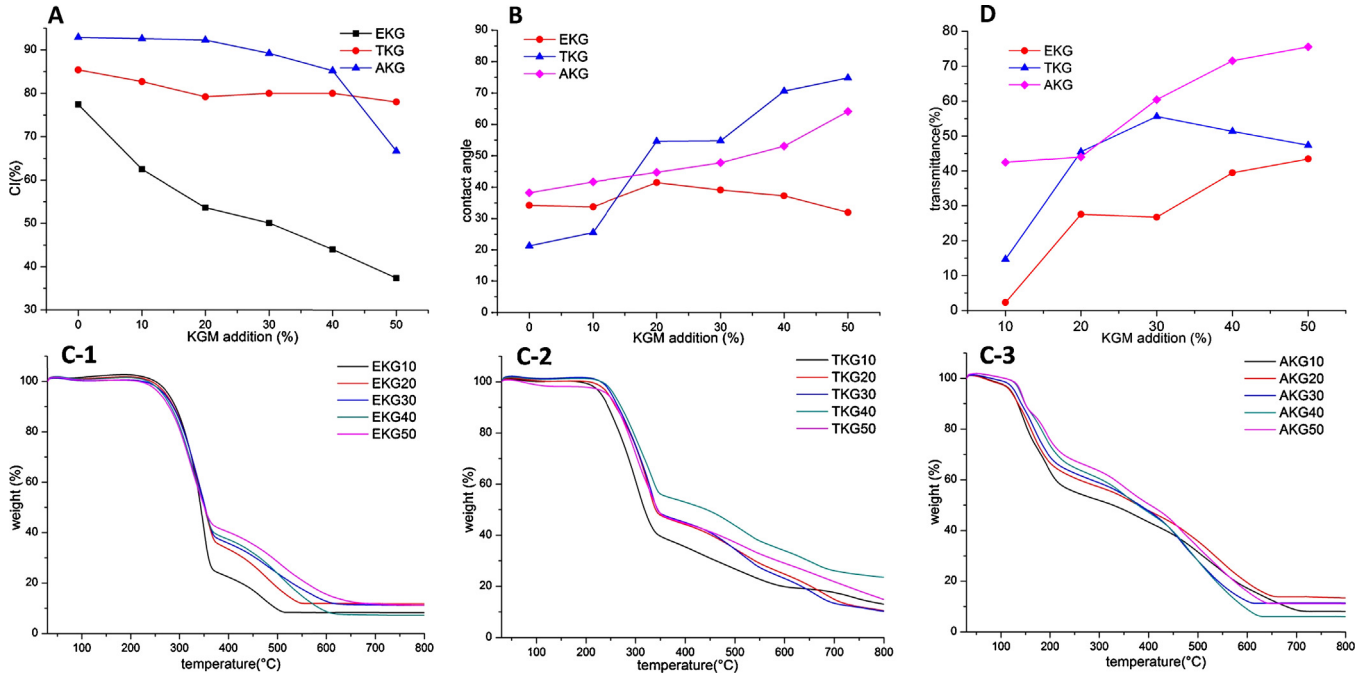

Fig. 4. Property changes of CN–KGM composite films with respect to the addition percentage of KGM. (A) Crystallinity index (CI); (B) contact angle; (C) thermal gravimetric analysis (TGA) graphs; (D) optical transmittance (at 600 nm).

Table 3
Mechanical strength of CN–GM composite films.

CN	GM	Composite film	Tensile strength (MPa)	Young's modulus (GPa)
ECN	KGM	EKG20	99.98 ± 44.09	12.12 ± 0.21
	SGM	ESG20	142.49 ± 31.23	17.12 ± 2.04
TCN	KGM	TKG50	55.56 ± 21.32	11.71 ± 1.37
	SGM	TSG50	169.21 ± 64.89	17.88 ± 4.38
ACN	KGM	AKG50	15.54 ± 6.91	3.87 ± 1.12
	SGM	ASG50	128.43 ± 54.91	16.58 ± 3.55
Regenerated TC	KGM	CKG10	32.53 ± 10.18	0.51 ± 0.06
	SGM	CSG10	39.99 ± 28.12	0.50 ± 0.18

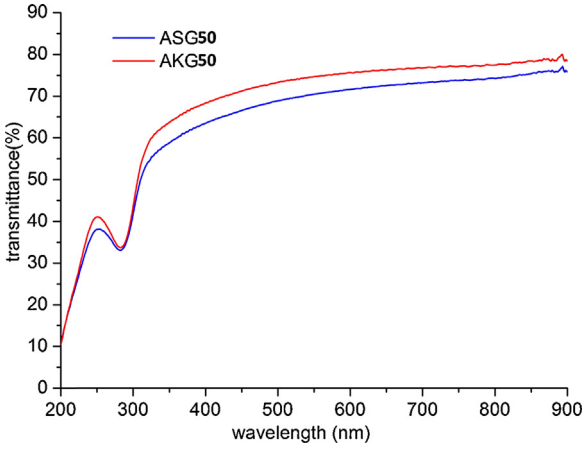

Fig. 5. Optical transmittance curves of AKG50 and ASG50 composite films.

3.5.2. Optical property

Due to the cement effect of GM, the transmittance at 600 nm increased as the percentage of KGM increased from 10% to 50% for the CN–KGM composite films and from 5%, 17% and 38% to 33%, 52% and 73% for the EKG, TKG and AKG films, respectively (Fig. 4(D)). This observation could be due to the fact that as the percentage of KGM increases, the film surface became smoother; thus, the light reflection caused by the rough surface was reduced and the transmittance increased.

Although the chiral nematic order phenomenon of CN films (Capadona et al., 2007) has not been investigated in detail in this study, special light reflection was observed for the ACN–KGM and ACN–SGM composite films, where the transmittance at a wavelength of approximately 300 nm was sharply reduced (Fig. 5).

3.5.3. Mechanical strength

The tensile strength and Young's modulus of the CN–KGM composite films increased in the order of ACN < TCN < ECN (15.54 MPa and 3.87 GPa, 55.56 MPa and 11.71 GPa and 99.98 MPa and 12.12 GPa, respectively) (Table 3). This order is consistent with the order of the aspect ratio of the CNs after different preparation treatments, indicating that the aspect ratio is a decisive factor for the mechanical properties of the composite films. The higher the aspect ratio of the CN, the more rigid the filler network and the more reinforcement present in the composite system. This finding was previously reported in another study (Fujisawa, Ikeuchi, Takeuchi, Saito, & Isogai, 2012).

Compared with the CN–KGM composite films, the CN–SGM composite films with the same GM percentage exhibited better mechanical properties and more rigidity, as demonstrated by their higher tensile strength (128.43–169.21 MPa) and Young's modulus (16.58–17.88 GPa). This difference could be the result of the difference in GM molecular masses, 10k for SGM and 1000k for KGM. With much lower molecular masses, SGM displayed better penetration into the CN network, better reinforcing the interactions with the CN to form a stronger network. This is supported by the fibril width differences observed as discussed in Section 3.4. We cannot rule out the idea that the higher mannose/glucose ratio in SGM compared to KGM (3.75 vs. 1.46) could allow for better hydrogen bond formation between the mannose structure and the CN; thus, the network cemented by SGM was stronger. In the structures, the hydroxyl groups at C-2 and C-3 in mannose demonstrate a *cis*-configuration, compared to the *trans*-configuration observed for glucose. Therefore, their ability to form intermolecular hydrogen bonds should be different. The best mechanical strengths were observed for the TCN–SGM film TSG50, with a tensile strength and Young's modulus of 169.21 MPa and 17.88 GPa, respectively. There is a possibility that in the case of TCN–SGM, strong hydrogen bondings may have been formed between the carboxylic acid from TCN and the diol part of mannose from SGM.

To our knowledge, this is specifically the first study to systematically report the preparation, structure and high mechanical strength of tunicate CN–GM nanocomposite films, especially for using SGM. In the literature, TC whiskers have been tested for their ability to reinforce starch films. However, the reported maximum tensile strength of ~15 MPa and Young's modulus of 315 MPa (Anglès & Dufresne, 2001) were much lower than those observed in this work. Compared with the mechanical properties of similar composite films prepared from woody cellulose and KGM (tensile strength of 57–107 MPa (Guang et al., 1998), 32–58 MPa (Yang, Xiong, & Zhang, 2002), 70 MPa (Cheng, Abd Karim, Norziah, & Seow, 2002), or 110 MPa (Yu, Jiang, Zou, Duan, & Xiong, 2009) and Young's modulus of 3 GPa (Cheng, Abd Karim, & Seow, 2008) or 3.6 GPa (Cheng et al., 2002) or from woody CN and spruce galactoglucomannan (tensile strength of ~10 MPa and Young's modulus of 500 MPa (Cheng et al., 2002) reported by other researchers, the composite films prepared in this study showed apparently better mechanical properties. Though even higher Young's modulus (28–50 GPa) and tensile strength (1.47–1.94 GPa) were reported for PVA-TC whiskers composites (Uddin et al., 2011; Uddin, Fujie, Sembo, & Gotoh, 2012), these studies were however based on extremely oriented TC whiskers which certainly could supply higher reinforcing effect than the randomly orientated CNs reported in this study.

As a reference experiment, CKG10 and CSG10 were prepared by the ionic liquid method after blending TC with 10% KGM and SGM, and very flexible composite films were obtained. This characteristic was achieved because the TC crystalline structure was largely destroyed by the ionic liquid dissolution. However, the films showed lower tensile strength and Young's Modulus than other CN–GM films (Table 3) due to the elimination of the crystalline structure, confirming that the cellulose crystal structure is essential for the films' mechanical behaviour.

4. Conclusions

From the same starting tunicate cellulose obtained from *Ciona intestinalis*, three different processing methods were used to produce three different cellulose nanocrystals (CNs) in terms of chemical and morphological structures (especially regarding the differences in their molecular masses, aspect ratios and amounts

of surface charge). Neat CN films were formed after fibril self-assembly, where stiff crystals packed with each other after orientation to avoid self-repulsion (e.g., fibrils tended to be parallel to each other in charged CNs and after structural densification due to the formation of intermolecular hydrogen bonds). CNs and glucomannan (GM) are two natural polymers that are compatible in combination and form strong interactions. Therefore, new mixed crystals consisting of CN fibrils cemented by GM were formed during the fabrication process due to the similarity of the two polymers. Consequently, a reinforced network was constructed in the CN–GM nanocomposite films. The composite films showed excellent mechanical properties, with high tensile strength and Young's modulus. The best mechanical strengths were observed for the 50–50% blended TCN-spruce GM film. The films also displayed good optical transparency and thermal stability. Therefore, these inherently edible polymeric films could substitute for non-biodegradable films in the food or pharmaceutical industries. Further study in this area should focus on optical and barrier properties.

Acknowledgements

We would like to acknowledge the China Scholarship Council (CSC) for supporting the studies of Yadong Zhao and Yujia Zhang's Ph.D. at KTH. Christofer Troedsson, Eric Thompson and Jean-Marie Bouquet from University of Bergen are acknowledged for the collection of tunicate samples in Norway. Jasna S. Stevanic and Lennart Salmén from Innventia are acknowledged for dynamic FTIR analysis.

References

Anglès, M. N., & Dufresne, A. (2000). Plasticized starch/tunicin whiskers nanocomposites. 1. Structural analysis. *Macromolecules*, *33*(22), 8344–8353.

Anglès, M. N., & Dufresne, A. (2001). Plasticized starch/tunicin whiskers nanocomposite materials. 2. Mechanical behavior. *Macromolecules*, *34*(9), 2921–2931.

Araki, J., Wada, M., & Kuga, S. (2000). Steric stabilization of a cellulose microcrystal suspension by poly(ethylene glycol) grafting. *Langmuir*, *17*(1), 21–27.

Ayranci, E., & Tunç, S. (1997). Cellulose-based edible films and their effects on fresh beans and strawberries. *Zeitschrift für Lebensmitteluntersuchung und Forschung A*, *205*(6), 470–473.

Azizi Samir, M. A. S., Alloin, F., & Dufresne, A. (2005). Review of recent research into cellulosic whiskers, their properties and their application in nanocomposite field. *Biomacromolecules*, *6*(2), 612–626.

Besbes, I., Alila, S., & Boufi, S. (2011). Nanofibrillated cellulose from TEMPO-oxidized eucalyptus fibres: Effect of the carboxyl content. *Carbohydrate Polymers*, *84*(3), 975–983.

Capadona, J. R., Van Den Berg, O., Capadona, L. A., Schroeter, M., Rowan, S. J., Tyler, D. J., et al. (2007). A versatile approach for the processing of polymer nanocomposites with self-assembled nanofibre templates. *Nature Nanotechnology*, *2*(12), 765–769.

Chang, C. P., Wang, I. C., Hung, K. J., & Perng, Y. S. (2010). Preparation and characterization of nanocrystalline cellulose by acid hydrolysis of cotton linter. *Taiwan Journal of Forest Science*, *25*(3), 251–264.

Cheng, L. H., Abd Karim, A., Norziah, M. H., & Seow, C. C. (2002). Modification of the microstructural and physical properties of konjac glucomannan-based films by alkali and sodium carboxymethylcellulose. *Food Research International*, *35*(9), 829–836.

Cheng, L. H., Abd Karim, A., & Seow, C. C. (2008). Characterisation of composite films made of konjac glucomannan (KGM), carboxymethyl cellulose (CMC) and lipid. *Food Chemistry*, *107*(1), 411–418.

de Souza Lima, M. M., & Borsali, R. (2004). Rodlike cellulose microcrystals: Structure, properties, and applications. *Macromolecular Rapid Communications*, *25*(7), 771–787.

Dufresne, A., Kellerhals, M. B., & Witholt, B. (1999). Transcrystallization in Mcl-PHAs/cellulose whiskers composites. *Macromolecules*, *32*(22), 7396–7401.

Elazzouzi-Hafraoui, S., Nishiyama, Y., Putaux, J.-L., Heux, L., Dubreuil, F., & Rochas, C. (2007). The shape and size distribution of crystalline nanoparticles prepared by acid hydrolysis of native cellulose. *Biomacromolecules*, *9*(1), 57–65.

Favier, V., Canova, G. R., Cavaillé, J. Y., Chanzy, H., Dufresne, A., & Gauthier, C. (1995). Nanocomposite materials from latex and cellulose whiskers. *Polymers for Advanced Technologies*, *6*(5), 351–355.

Fernandes, S. C. M., Freire, C. S. R., Silvestre, A. J. D., Pascoal Neto, C., Gandini, A., Berglund, L. A., et al. (2010). Transparent chitosan films reinforced with a high content of nanofibrillated cellulose. *Carbohydrate Polymers*, *81*(2), 394–401.

Fleming, K., Gray, D. G., & Matthews, S. (2001). Cellulose crystallites. *Chemistry*, *7*(9), 1831–1835.

Fujisawa, S., Ikeuchi, T., Takeuchi, M., Saito, T., & Isogai, A. (2012). Superior reinforcement effect of TEMPO-oxidized cellulose nanofibrils in polystyrene matrix: Optical, thermal, and mechanical studies. *Biomacromolecules*, *13*(7), 2188–2194.

Guang, Y., Lina, Z., Yamane, C., Miyamoto, I., Inamoto, M., & Okajima, K. (1998). Blend membranes from cellulose/konjac glucomannan cuprammonium solution. *Journal of Membrane Science*, *139*(1), 47–56.

Habibi, Y., Chanzy, H., & Vignon, M. (2006). TEMPO-mediated surface oxidation of cellulose whiskers. *Cellulose*, *13*(6), 679–687.

Habibi, Y., Lucia, L. A., & Rojas, O. J. (2010). Cellulose nanocrystals: Chemistry, self-assembly, and applications. *Chemical Reviews*, *110*(6), 3479–3500.

Henriksson, M., Henriksson, G., Berglund, L. A., & Lindström, T. (2007). An environmentally friendly method for enzyme-assisted preparation of microfibrillated cellulose (MFC) nanofibers. *European Polymer Journal*, *43*(8), 3434–3441.

Hirose, E., Kimura, S., Itoh, T., & Nishikawa, J. (1999). Tunic morphology and cellulosic components of pyrosomas, doliolids, and salps (Thaliacea, Urochordata). *The Biological Bulletin*, *196*(1), 113–120.

Jiang, F., & Hsieh, Y.-L. (2013). Chemically and mechanically isolated nanocellulose and their self-assembled structures. *Carbohydrate Polymers*, *95*(1), 32–40.

Kimura, S., & Itoh, T. (2007). Biogenesis and function of cellulose in the tunicates. In R. M. Brown Jr., & I. Saxena (Eds.), *Cellulose: Molecular and structural biology* (pp. 217–236). Netherlands: Springer.

Kimura, S., Ohshima, C., Hirose, E., Nishikawa, J., & Itoh, T. (2001). Cellulose in the house of the appendicularian *Oikopleura rufescens*. *Protoplasma*, *216*(1–2), 71–74.

Klemm, D., Heublein, B., Fink, H. P., & Bohn, A. (2005). Cellulose: fascinating biopolymer and sustainable raw material. *Angewandte Chemie International Edition English*, *44*(22), 3358–3393.

Li, B., & Xie, B. J. (2006). Single molecular chain geometry of konjac glucomannan as a high quality dietary fiber in East Asia. *Food Research International*, *39*(2), 127–132.

Łojewska, J., Miśkowiec, P., Łojewski, T., & Proniewicz, L. M. (2005). Cellulose oxidative and hydrolytic degradation: In situ FTIR approach. *Polymer Degradation and Stability*, *88*(3), 512–520.

Mikkonen, K., Mathew, A., Pirkkalainen, K., Serimaa, R., Xu, C., Willför, S., et al. (2010). Glucomannan composite films with cellulose nanowhiskers. *Cellulose*, *17*(1), 69–81.

Moon, R. J., Martini, A., Nairn, J., Simonsen, J., & Youngblood, J. (2011). Cellulose nanomaterials review: Structure, properties and nanocomposites. *Chemical Society Reviews*, *40*(7), 3941–3994.

Okita, Y., Fujisawa, S., Saito, T., & Isogai, A. (2010). TEMPO-oxidized cellulose nanofibrils dispersed in organic solvents. *Biomacromolecules*, *12*(2), 518–522.

Okita, Y., Saito, T., & Isogai, A. (2010). Entire surface oxidation of various cellulose microfibrils by TEMPO-mediated oxidation. *Biomacromolecules*, *11*(6), 1696–1700.

Peng, B. L., Dhar, N., Liu, H. L., & Tam, K. C. (2011). Chemistry and applications of nanocrystalline cellulose and its derivatives: A nanotechnology perspective. *The Canadian Journal of Chemical Engineering*, *89*(5), 1191–1206.

Persson, T., Nordin, A. K., Zacchi, G., & Jonsson, A. S. (2007). Economic evaluation of isolation of hemicelluloses from process streams from thermomechanical pulping of spruce. *Applied Biochemistry and Biotechnology*, *137–140*(1–12), 741–752.

Reddy, N., & Yang, Y. (2005). Structure and properties of high quality natural cellulose fibers from cornstalks. *Polymer*, *46*(15), 5494–5500.

Revol, J. F., Bradford, H., Giasson, J., Marchessault, R. H., & Gray, D. G. (1992). Helicoidal self-ordering of cellulose microfibrils in aqueous suspension. *International Journal of Biological Macromolecules*, *14*(3), 170–172.

Ruiz, M. M., Cavaillé, J. Y., Dufresne, A., Graillat, C., & Gérard, J.-F. (2001). New waterborne epoxy coatings based on cellulose nanofillers. *Macromolecular Symposia*, *169*(1), 211–222.

Rusli, R., Shanmuganathan, K., Rowan, S. J., Weder, C., & Eichhorn, S. J. (2011). Stress transfer in cellulose nanowhisker composites—Influence of whisker aspect ratio and surface charge. *Biomacromolecules*, *12*(4), 1363–1369.

Sorrentino, A., Gorrasi, G., & Vittoria, V. (2007). Potential perspectives of bionanocomposites for food packaging applications. *Trends in Food Science & Technology*, *18*(2), 84–95.

Stevanic, J., Bergström, E., Gatenholm, P., Berglund, L., & Salmén, L. (2012). Arabinoxylan/nanofibrillated cellulose composite films. *Journal of Materials Science*, *47*(18), 6724–6732.

Stevanic, J. S., & Salmén, L. (2009). Orientation of the wood polymers in the cell wall of spruce wood fibres. *Holzforschung*, *63*, 497–503.

Šturcová, A., Davies, G. R., & Eichhorn, S. J. (2005). Elastic modulus and stress-transfer properties of tunicate cellulose whiskers. *Biomacromolecules*, *6*(2), 1055–1061.

Teixeira, E. d. M., Pasquini, D., Curvelo, A. A. S., Corradini, E., Belgacem, M. N., & Dufresne, A. (2009). Cassava bagasse cellulose nanofibrils reinforced thermoplastic cassava starch. *Carbohydrate Polymers*, *78*(3), 422–431.

Uddin, A. J., Araki, J., & Gotoh, Y. (2011). Extremely oriented tunicin whiskers in poly(vinyl alcohol) nanocomposites. *Polymer International*, *60*(8), 1230–1239.

Uddin, A. J., Fujie, M., Sembo, S., & Gotoh, Y. (2012). Outstanding reinforcing effect of highly oriented chitin whiskers in PVA nanocomposites. *Carbohydrate Polymers*, *87*(1), 799–805.

Veigel, S., Müller, U., Keckes, J., Obersriebnig, M., & Gindl-Altmutter, W. (2011). Cellulose nanofibrils as filler for adhesives: Effect on specific fracture energy of solid wood-adhesive bonds. *Cellulose*, *18*(5), 1227–1237.

Whitney, S. E. C., Brigham, J. E., Darke, A. H., Reid, J. S. G., & Gidley, M. J. (1998). Structural aspects of the interaction of mannan-based polysaccharides with bacterial cellulose. *Carbohydrate Research*, *307*(3–4), 299–309.

Yang, G., Xiong, X., & Zhang, L. (2002). Microporous formation of blend membranes from cellulose/konjac glucomannan in NaOH/thiourea aqueous solution. *Journal of Membrane Science*, *201*(1–2), 161–173.

Yu, Z., Jiang, Y., Zou, W., Duan, J., & Xiong, X. (2009). Preparation and characterization of cellulose and konjac glucomannan blend film from ionic liquid. *Journal of Polymer Science B: Polymer Physics*, *47*(17), 1686–1694.

Yuan, Z. H., Wu, D. C., Zhao, Y., Wu, H., & Li, X. Y. (2003). The determination of konjac glucomannan in konjac refined powder and monosaccharide compositions by HPLC. *Zhongguo Zhong Yao Za Zhi*, *28*(7), 621–624.

Zhang, L., Liu, H., Zheng, L., Zhang, J., Du, Y., & Feng, H. (1996). Biodegradability of regenerated cellulose films in soil. *Industrial & Engineering Chemistry Research*, *35*(12), 4682–4685.

Zhang, Y., Li, J., Lindström, M. E., Stepan, A., & Gatenholm, P. (2013). Spruce glucomannan: preparation, purification, characterization and derivatization. *Nordic Pulp & Paper Research Journal*, *28*, 478–483.

Zhao, Y., & Li, J. (2014). Excellent chemical and material cellulose from tunicates: diversity in cellulose production yield and chemical and morphological structures from different tunicate species. *Cellulose*, *21*(5), 3427–3441.